Received: Added at production | Revised: Added at production | Accepted: Added at production

DOI: xxx/xxxx

RESEARCH ARTICLE

# LIDAR-assisted feedforward individual pitch control of a 15 MW floating offshore wind turbine

**Andrew J. Russell**[1] | **Maurizio Collu**[2] | **Alasdair S. McDonald**[3] | **Philipp R. Thies**[4] | **Aidan Keane**[5] | **Alexander R. Quayle**[6]

[1]Industrial Doctoral Centre for Offshore Renewable Energy, School of Engineering, King's Buildings, University of Edinburgh, Edinburgh, EH9 3JL, UK

[2]Department of Naval Architecture, Ocean and Marine Engineering, University of Strathclyde, 100 Montrose St, Glasgow, G4 0LZ, UK

[3]School of Engineering, King's Buildings, University of Edinburgh, Edinburgh, EH9 3JL UK

[4]Faculty of Environment, Science and Economy Engineering, University of Exeter, Penryn Campus, TR10 9FE, UK

[5]Wood Renewables, Floor 2 St Vincent Plaza, St Vincent Street, Glasgow, G2 5LP, UK

[6]Flotation Energy Ltd, 12 Alva Street, Edinburgh, EH2 4QG, UK

**Correspondence**
Andrew J. Russell,
Email: A.J.Russell-1@sms.ed.ac.uk

## Abstract

Nacelle-mounted, forward-facing LIDAR technology is able to deliver benefits to rotor speed regulation and loading reductions of floating offshore wind turbines when assisting with blade pitch control in above-rated wind speed conditions. Large-scale wind turbines may be subject to significant variations in structural loads due to differences in the wind profile across the rotor-swept area. These loading fluctuations can be mitigated through the use of individual blade pitch control (IPC). This paper presents a novel LIDAR-assisted feedforward IPC approach that uses each blade's rotor azimuth position to allocate an appropriate individual pitch command from a multi-beam LIDAR. In this computational study, the source code of OpenFAST wind turbine modelling software was modified to enable LIDAR simulation and LIDAR-assisted control. The LIDAR simulation modifications made are present in the latest OpenFAST release, v3.5. Simulations were performed on a single 15 MW floating offshore wind turbine across the above-rated wind spectrum and using multiple randomly generated wind profiles. Under a turbulent wind field with an average wind speed of 17 $ms^{-1}$, the LIDAR-assisted feedforward IPC delivered root mean squared error and standard deviation reductions to key turbine and substructure parameters by up to 35%. Feedforward IPC delivered enhancements of up to 10% over feedforward collective pitch control, which instead provided the same feedforward command to all blades, compared to the baseline feedback controller. The reductions to the standard deviation and range of the rotor speed may enable structural optimisation of the tower, while the reductions in the variations in the loadings present an opportunity for reduced fatigue damage on turbine components and, consequently, a reduction in maintenance expenditure.

**KEYWORDS**
LIDAR-assisted control, Feedforward Control, Nacelle Mounted LIDAR, Individual Pitch Control

## 1 | INTRODUCTION

The application of light detection and ranging (LIDAR) technology for assisting wind turbine control is gathering momentum in its path towards commercialisation. Nacelle-mounted, forward-facing LIDAR can provide measurements of the incoming wind field, the characteristics of which can be used for feedforward turbine control. Traditionally, wind turbine control strategies have utilised feedback control, which updates the controller settings following the impact of the incoming disturbance. However, the drawback of this type of control strategy is that the wind turbine controller provides a delayed reaction to the incoming wind. Feedforward control is able to overcome this drawback by enabling turbines to actuate their torque, pitch or yaw systems in advance of the wind's impact upon the rotor.

According to the existing literature, the greatest benefits delivered by LIDAR-assisted control have been achieved when assisting with blade pitch control in above-rated conditions[1, 2, 3]. LIDAR-assisted feedforward pitch control is able to enhance turbine performance through improved rotor speed regulation, and therefore more stable power capture. It is also capable of reducing the variation in the structural loadings, which has the potential to reduce the levelised cost of offshore wind energy by extending maintenance intervals and the lifetime of wind turbines.

  

Floating offshore wind turbines are able to capture wind power from further distances offshore, where waters are too deep for the use of bottom-fixed turbines. However, as floating offshore wind turbines are subject to softer foundation properties, their control systems have to be designed differently from their bottom-fixed counterparts, primarily to prevent negative aerodynamic damping as a consequence of unfavourable coupling between the platform motion and the blade pitch controller in above-rated wind speeds[4,5]. These modifications give rise to greater rotor speed variation of floating offshore wind turbines compared to bottom-fixed turbines[4,6], resulting in larger rotor rotational (1P) and blade passing (3P) frequency ranges, and leading to the requirement for larger, stiffer turbine towers.

Within the literature, LIDAR-assisted pitch control has also demonstrated its ability to deliver reductions to the variations of the rotor speed, structural loads and platform motions of floating offshore wind turbines. Studies have focused on floating offshore wind turbines using spar-buoy[1] and tension-leg platform[2] foundations supporting the National Renewable Energy Laboratory (NREL)'s 5 MW reference turbine, as defined by Jonkman et al[7], and semi-submersible foundations for a 10 MW turbine model[3]. By 2024, turbines of up to 16 MW capacity will be commercially available[8]. Studies have now begun to predict the benefits attainable for these large floating turbines through simulations of LIDAR-assisted pitch control applied to the International Energy Agency (IEA)-Wind 15 MW reference turbine[9] mounted on the University of Maine's VolturnUS-S[10] semi-submersible platform[11,12].

Individual blade pitch control aims to mitigate the cyclic loads experienced by wind turbines due to variations in the wind profile across the rotor-swept area caused by wind shear, wind veer and turbulence. The concept of feedback IPC (FBIPC) was first explored by Bossanyi et al[13], and applied to floating turbines by Namik and Stol[14]. Within this strategy, the individual controller requires the three out-of-plane blade root bending moments and the rotor azimuth as feedback inputs to allow for the derivation of a pitch command for each blade, which adds to the collective command provided by the collective pitch controller.

Alternatively, feedforward individual pitch control (FFIPC), is able to deliver individual pitch commands in advance of the wind's impact and has been studied using various implementations[15,16,17,18]. Schlipf et al[15] used $H_\infty$ optimisation to design an individual pitch controller using a linear time-invariant (LTI) model. Raach et al[16] used a non-linear model predictive controller (NMPC) to deliver individual blade feedforward commands to a 5 MW floating wind turbine. Dunne et al[17,18] studied a LIDAR whose beams rotated with the blades, and was used to assign a command to each blade using the same proportional-integral (PI) controller as was used for the collective pitch controller. The LIDAR used three wind speed inputs, one at each blade, at approximately 75% span to deliver the individual commands and resulted in improvements over the baseline feedback individual pitch controller[18]. Studies are yet to investigate the benefits of LIDAR-assisted FFIPC of large (15 MW+) floating offshore wind turbines, whose rotor diameters are approaching 250 m. These large diameters will give rise to greater variations in the wind speed across the rotor-swept area, leading to significant variations in the loadings on the turbine's structures.

This paper aims to quantify the performance improvements and motion and loading reductions achievable through simulations of LIDAR-assisted pitch control of a 15 MW semi-submersible floating offshore wind turbine in above-rated wind speed conditions. The source code of OpenFAST wind turbine modelling software was modified to allow for the simulation of nacelle-mounted LIDAR wind velocity measurement. These modifications are present in the latest release of OpenFAST, v3.5[19]. Furthermore, the LIDAR measurements were interfaced with OpenFAST's control framework to enable LIDAR-assisted control within the Reference Open Source Controller (ROSCO)[20], which was also modified within this work. A multi-beam LIDAR was simulated to enable calculation of the rotor-effective wind speed (REWS), representing the average wind speed across the rotor-swept area. The REWS was used by the implemented feedforward controller, which included collective pitch control (CPC) and IPC capabilities. The FFIPC approach used the rotor azimuth position of each blade to allocate an appropriate individual pitch command, which was combined with the command provided by the feedforward-feedback collective pitch controller (FFCPC). Simulations were performed on a standalone 15 MW semi-submersible floating offshore wind turbine. The time series performance of the FFCPC, the FFCPC with traditional feedback individual pitch control (FFCPC+FBIPC) and the FFCPC with feedforward individual pitch control (FFCPC+FFIPC) was compared to that of the traditional feedback-only collective pitch controller (FB), which was used as the baseline. The impact of the rotor radius percentage span locations of the LIDAR beams on the performance of the FFCPC+FFIPC was also assessed. Performance benefits were quantified through comparison of normalised values of key performance metrics of various turbine and substructure parameters.

The paper is outlined as follows: Sect. 2 describes the modelling software, turbine and substructure models analysed. Sect. 3 outlines the modifications made to the OpenFAST and ROSCO source code to enable LIDAR measurement and control. Sect. 4 details the feedback and feedforward collective and individual pitch control theory. Sect. 5 describes the simulation setup and the key statistical metrics. Sect. 6 outlines the results, provides discussion on them and details the limitations of the study and Sect. 7 offers conclusions from the study and the next steps of the research.

# 2 | TURBINE-SUBSTRUCTURE MODELLING

This section provides information regarding the software, turbine and supporting structure used when performing the simulations. Furthermore, detail is provided on how the simulations were configured and how feedforward control was implemented.

## 2.1 | OpenFAST

The numerical modelling tool employed for this study was NREL's open-source Fatigue, Aerodynamics, Structures, and Turbulence (FAST) code. This software is classed as an aero-hydro-servo-elastic tool for the modelling of full nonlinear wind turbine models. It allows for the intricate specification of the turbine's design, external environment (wind, wave and current conditions) and the controller design. OpenFAST is the latest iteration of the FAST code and v3.4 was the original (before modifications) version of the program used in this study[21].

## 2.2 | Turbine and support structure models

### 2.2.1 | Turbine

The turbine studied in this work was the IEA-Wind 15 MW reference turbine, developed between NREL and the Technical University of Denmark (DTU), via the IEA, as defined by Gaertner et al[9]. The specifications of the reference turbine are given in Table 1.

**TABLE 1** Parameters of the IEA-Wind 15 MW reference turbine[9].

| Parameter | Value | Units |
|---|---|---|
| Power rating | 15 | MW |
| Turbine class | IEC Class B | - |
| Cut-in wind speed | 3 | $ms^{-1}$ |
| Rated wind speed | 10.59 | $ms^{-1}$ |
| Cut-out wind speed | 25 | $ms^{-1}$ |
| Design tip-speed ratio | 9.0 | - |
| Minimum rotor speed | 5.0 | rpm |
| Maximum rotor speed | 7.56 | rpm |
| Rotor diameter | 240 | m |
| Hub height | 150 | m |
| Drive train | Direct drive | - |

The turbine rotor operates with a minimum rotational speed of 5 rpm to avoid 3P interference with the tower/monopile natural frequencies[9], and reaches a rated rotational speed of 7.56 rpm at 10.59 $ms^{-1}$. The blades begin pitching at the rated wind speed in order to maintain the rotor rotation at its rated speed.

The baseline feedback controller used by the IEA-Wind 15 MW reference wind turbine is ROSCO, as described by Abbas et al[20]. A modified version of ROSCO v2.6 was used in this study. ROSCO uses a gain-scheduled feedback proportional-integral pitch controller in above-rated wind speed conditions. The ROSCO controller is typically packaged into a dynamic link library (.dll) file to be called by the ServoDyn (control) file.

### 2.2.2 | Substructure

The floating substructure model utilised for this work was the University of Maine (UMaine)'s VolturnUS-S semi-submersible[10], designed to support the IEA 15 MW reference wind turbine. Key specifications of the substructure are shown in Table 2.

### 2.2.3 | Tower

The towers of floating offshore wind turbines are required to have higher stiffness characteristics than bottom fixed configurations due to increased inertial and gravity loads resulting from platform motions[10]. Therefore, the tower for the VolturnUS-S was designed separately from the

**TABLE 2** Parameters of the VolturnUS-S semi-submersible model[10].

| Parameter | Value | Units |
|---|---|---|
| Material | Steel | - |
| Draft | 20 | m |
| Mass (including ballast) | 17,839 | kg |
| Mooring system | Three line catenary | - |

configuration of the monopile outlined by Gaertner et al[9]. The tower was designed to have its first fore-aft and side-to-side natural frequencies outside of the 1P and 3P ranges. The 1P and 3P ranges were modified for the 15 MW turbine on the VolturnUS-S to account for the increased rotor speed variation caused by the platform motions. Therefore, a stiff-stiff tower, with 1$^{st}$ natural frequencies above 3P was required because of a very narrow soft-stiff range between 1P and 3P when additional safety factors were applied[10]. Further detail on the tower design for the 15 MW VolturnUS-S can be found within its definition document[10].

# 3 | INTEGRATION OF LIDAR SIMULATION AND FEEDFORWARD CONTROL WITHIN OPENFAST

In the original version of OpenFAST v3.4 used in this study, LIDAR simulation was not possible within the program itself. Work has been conducted by Schlipf et al[22] and Guo et al[23] to develop an additional LIDAR simulator module to be called by the OpenFAST input file, with an additional .dll chain created for interface with the ROSCO controller. However, within this work, a LIDAR simulator has been developed that is integrated within the original OpenFAST framework. Here, LIDAR simulation is incorporated within the InflowWind module. The modifications made to OpenFAST (as will be outlined in Sect. 3.1) were proposed to NREL via a GitHub pull request. They were subsequently accepted and are present in the latest release of the program, v3.5[19]. The LIDAR measurements are linked with ServoDyn to enable interface with the modified ROSCO controller, developed to include LIDAR-assisted control. This section outlines the modifications made to the OpenFAST and ROSCO source code to allow for the integration of LIDAR simulation and LIDAR-assisted control.

## 3.1 | Integration of LIDAR simulation within InflowWind

As the InflowWind module of OpenFAST specifies the input wind conditions, it was identified as the point of integration of the LIDAR model. This was achieved through modification and addition to the source code, which is written in FORTRAN. Firstly, the source code was modified to allow for the LIDAR parameters and configuration to be specified within the InflowWind input file, allowing for customisation by the user. The input files are then parsed and saved as parameters within the source code to be used within the program.

The LIDAR beam(s) can be configured in multiple ways. Single-point beam(s) can be configured where focal distances can be specified independently for each beam. Alternatively, a single beam can be configured in a continuous or pulsed manner. In the continuous mode, a single focal distance is configured, whereas, in the pulsed mode, measurements can be taken at multiple range gates. In both continuous and pulsed configurations, the beam is modelled as a Gaussian beam, whereby a weighting function defines the probe length at the focal point. The measurement frequency can also be specified. Additionally, the simulator can account for the impacts of platform motions on the movement of the nacelle, which are extracted from the ElastoDyn module. These can be used to modify the measurement coordinates of the LIDAR beam(s).

The LIDAR device's wind speed measurements are taken from the wind field provided to InflowWind such as those generated by TurbSim. The LIDAR's wind speed measurements can be outputted from the InflowWind module for user analysis and for interface with other modules, such as ServoDyn, for LIDAR-assisted control. The authors are aware that the method used to determine the previewed wind measurements are not wholly representative of a real LIDAR system. In reality, the LIDAR would measure a projection of the wind velocity onto the LIDAR beam's direction. In this case, a wind field model would have to be invoked and the wind velocity would be reconstructed with a wind field reconstruction method (WFR), as is the case in works published by Schlipf et al[22] and Guo et al[23, 24]. In addition, it has been assumed that the wind velocity does not change from the point of measurement to the rotor, therefore assuming Taylor's frozen hypothesis[25]. In reality, the wind velocity would evolve in this interval, though previous studies have considered the wind evolution and found it to not be significantly impactful on the performance of LIDAR-assisted control, and that a simple linear filter design for LIDAR-assisted control is sufficient for various atmospheric stability conditions[24].

## 3.2 | Interface of LIDAR measurement to ROSCO

ServoDyn is the module within OpenFAST responsible for defining control inputs and outputs and calling to the requested controller interface, which is typically a .dll file, namely ROSCO. As ROSCO is compiled to a .dll using a separate FORTRAN solution to OpenFAST, an interface between the two is required so that inputs and outputs can be transferred. Within OpenFAST, this is achieved using the avrSWAP array, which is constructed within ServoDyn.

To achieve interface to the ServoDyn module from InflowWind, the LIDAR-measured wind speed outputs of the InflowWind module had to be specified as inputs within the ServoDyn module's source code, and these could then be added to the avrSWAP array to be sent to ROSCO.

The LIDAR-assisted collective pitch controller was created by adding an additional feedforward control subroutine within the ROSCO source code. The pitch controller calls the feedforward control script to compute the outputs to be sent to the feedforward-feedback controller for the determination of the pitch command. If individual feedforward pitch control is enabled, a further separate subroutine is called to compute the individual commands to be assigned to each blade.

# 4 | PITCH CONTROLLER THEORY

## 4.1 | Feedback pitch controller

If LIDAR-assisted control is disabled, the feedforward control subroutine is not used and only the feedback pitch controller is employed. Within ROSCO, this utilises a gain-scheduled proportional-integral controller. This requires the generator's rotational speed as the feedback input. The error between the low-pass filtered generator rotational speed ($\Omega_g$) and the rated generator rotational speed ($\Omega_{g,rated}$) is first calculated.

$$e_{FB} = \Omega_{g,rated} - \Omega_g \tag{1}$$

where $e_{FB}$ is the feedback generator rotational speed error. The proportional component of the feedback controller ($P_{FB}$) is then calculated through multiplication of $e_{FB}$ with a scheduled (according to the blade pitch angle) proportional gain term ($K_p$).

$$P_{FB} = K_p \, e_{FB} \tag{2}$$

The integral component of the feedback controller ($I_{FB}$) is calculated through multiplication of $e_{FB}$ with the time step duration ($dt$) and the gain-scheduled integral gain ($K_i$), which is added to the previous feedback integral component ($I_{FB,prev}$).

$$I_{FB} = I_{FB,prev} + dt(K_i \, e_{FB}) \tag{3}$$

The feedback pitch command ($\theta_{FB}$) is determined through combination of $P_{FB}$ and $I_{FB}$.

$$\theta_{FB} = P_{FB} + I_{FB} \tag{4}$$

For floating turbines, an additional pitch command is provided through consideration of the nacelle acceleration to aid in overcoming negative aerodynamic damping. The tower-top acceleration ($\ddot{x}_{tt}$) is measured and multiplied by a proportional feedback term ($K_{p,TFB}$) which is then combined with the command from the feedback pitch controller.

$$\theta_{TFB} = K_{p,TFB} \, \ddot{x}_{tt} \tag{5a}$$

$$\theta_{FB} = \theta_{FB} + \theta_{TFB} \tag{5b}$$

where $\theta_{TFB}$ is the tower-top feedback pitch command.

## 4.2 | Feedforward collective pitch controller

The feedforward control approach used a 5-beam LIDAR, with 4 beams focused around the rotor disk and one focused at hub height directly ahead of the turbine, as illustrated in Fig. 1.

When using a multiple-beam LIDAR, as in this study, the rotor effective wind speed (REWS) can be calculated, which represents the average wind speed across the rotor-swept area. In this study, this was determined by averaging the longitudinal wind speeds of the LIDAR measurement

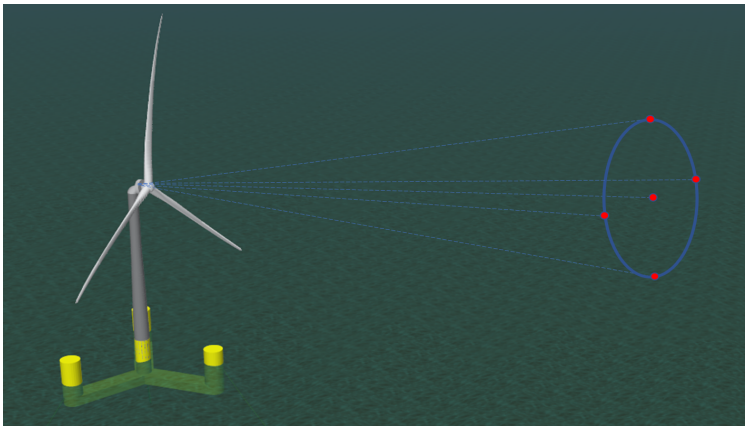

**FIGURE 1** Illustrating a side view of the nacelle-mounted LIDAR beam trajectories, marked by blue dashed lines, and their focal positions, marked by red dots. Not to scale.

points, which were evenly distributed across the rotor-swept area. This allowed for a more representative single wind speed value to be used by the controller.

$$REWS = \frac{\sum_{j=1}^{n_{beams}} v_{LIDAR,j}}{n_{beams}} \tag{6}$$

where $j$ is the beam number, $v_{LIDAR,j}$ is the longitudinal LIDAR measured wind speed of each beam and $n_{beams}$ is the number of LIDAR beams. The correct LIDAR REWS record to be used for the feedforward pitch command had to be recalled at the required time. This required accounting for the transport delay of the wind from the point of measurement to the turbine. This was achieved through the use of a buffer, and it was assumed that the measured wind did not evolve or change from the point of measurement to the turbine. Upon each new time step of the simulation, the values stored in the buffer were shifted across to vacate the first space of the array for the latest LIDAR REWS measurement. The current LIDAR REWS wind speed measurement was then passed through a first-order low-pass filter with the following transfer function:

$$G_{LPF}(s) = \frac{2\pi f_c}{s + 2\pi f_c} \tag{7}$$

where $f_c$ is the corner frequency specified in the ROSCO.IN input file. The gain, $G_{LPF}$, was applied to filter the LIDAR REWS wind speed measurement, which was then assigned to the first position within the buffer.

The approximate lead time of the current LIDAR measurement from the point of measurement to the turbine ($t_{l,1}$) was:

$$t_{l,1} = \frac{D_x}{v_f} \tag{8}$$

where $D_x$ is the x-direction focal distance (equal for all beams) and $v_f$ is the low-pass filtered LIDAR measured REWS. The time within the simulation at which the latest LIDAR wind speed measurement will reach the turbine was:

$$t_{impact,1} = t + t_{l,1} \tag{9}$$

where $t_{impact,1}$ is the time within the simulation that the current LIDAR measurement will impact upon the turbine and $t$ is the current simulation time. The impact time was also stored in a buffer vector housing estimated impact times for each LIDAR REWS record. Similarly to the REWS records, the latest impact time record assumed the first position after the previous records were shifted across. The two buffer vectors were aligned in their positions of the expected time of impact and the filtered LIDAR REWS. The specified pitch actuation preview time ($t_{pitch}$) and $t$ were then subtracted from each of the values in the impact time buffer vector, such that values stored in the vector decreased as time increased. $t_{pitch}$ was selected to ensure ample time to account for the delay incurred by the pitch actuators and the low-pass filter.

$$t_{interval,i} = t_{impact,i} - t - t_{pitch} \tag{10}$$

The location within the $t_{interval}$ vector that had a value closest to zero was then selected, and the value at the same location within the filtered LIDAR REWS vector was selected as the wind speed record to use when calculating the feedforward command for the current time step. The feedforward pitch angle ($\theta_{FF,setpoint}$) was then determined through interpolation of the wind speed-pitch angle curve specified in the ROSCO input file (Fig. 2).

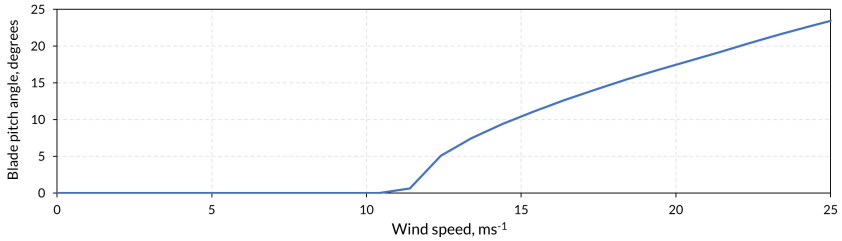


**FIGURE 2** Wind speed-blade pitch angle curve as used in the modified ROSCO input file.

The error ($e_{FF}$) between $\theta_{FF,setpoint}$ and the current average pitch angle of the turbine blades ($\theta_{c,avg}$) was computed.

$$e_{FF} = \theta_{FF,setpoint} - \theta_{c,avg} \tag{11}$$

The feedforward pitch command was then determined through multiplication with a proportional gain term ($K_{p,FF}$) which was tuned by trial and error.

$$\theta_{FF} = K_{p,FF}\, e_{FF} \tag{12}$$

The magnitude of $\theta_{FF}$ had to be limited at wind speeds close to the below-rated-to-above-rated transition because the blade pitch curve of the IEA 15 MW turbine increases steeply within the first few metres per second of the above-rated spectrum, as indicated in Fig. 2. Therefore, at wind speeds slightly above the rated wind speed, the feedforward controller was prone to giving disproportionately large commands, resulting in large spikes in blade pitch angle. Therefore, in wind speeds below 13 ms$^{-1}$, strict limits had to be imposed on the feedforward pitch commands to prevent these large spikes. This restriction was also acknowledged by Guo et al[24], who made the feedforward controller inactive in wind speeds below 14 ms$^{-1}$.

$\theta_{FF}$ was used in two ways. Firstly, the difference between $\theta_{FF}$ and the feedforward command computed at the previous time step ($\theta_{FF,prev}$) was calculated and divided by $dt$ to give the rate of change ($\dot{\theta}_{FF}$).

$$\dot{\theta}_{FF} = \frac{\theta_{FF} - \theta_{FF,prev}}{dt} \tag{13}$$

$\dot{\theta}_{FF}$ was then included within the calculation of $I_{FB}$ (Eq. 3). The feedforward rate addition methodology has also been applied in previous studies[1, 3, 24].

$$I_{FF\text{-}FB} = I_{FF\text{-}FB,prev} + dt\left(K_i(e_{FB}) + (\dot{\theta}_{FF})\right) \tag{14}$$

where $I_{FF-FB}$ is the feedforward modified feedback controller integral component and $I_{FF-FB,prev}$ is the value of $I_{FF-FB}$ computed at the previous time-step. $P_{FB}$ (from Equation 2) and $I_{FF-FB}$ were then combined to give the feedforward modified feedback pitch command. Here, $\theta_{FF}$ was then combined with the feedforward modified feedback pitch command and tower-top feedback ($\theta_{TFB}$) commands to give the feedforward-feedback pitch command ($\theta_{FF-FB}$).

$$\theta_{FF\text{-}FB} = (P_{FB} + I_{FF\text{-}FB}) + \theta_{TFB} + \theta_{FF} \tag{15}$$

## 4.3 | Feedback individual pitch controller

Simulations were performed combining FFCPC with FBIPC to enable comparison with those of FFCPC combined with the FFIPC strategy. The FBIPC approach used in this study, as defined by Bossanyi et al[13] and Magar et al[26] and configurable within ROSCO v2.6, uses the out-of-plane bending moment at the root of each blade and the rotor azimuth as its feedback inputs. Magar et al[26], likened the sinusoidal variation in the blade root bending moments (caused by the vertical wind shear) of three-bladed horizontal axis wind turbines, whose blades are positioned 120° apart, to that of the three-phase system used in the electrical power systems. To suppress this variation, the FBIPC could vary the individual blade pitch according to

$$\theta_1 = \theta_{avg}\, cos(A) \tag{16a}$$

$$\theta_2 = \theta_{avg}\, cos\left(A + \frac{2\pi}{3}\right) \tag{16b}$$

$$\theta_3 = \theta_{avg}\, cos\left(A + \frac{4\pi}{3}\right) \tag{16c}$$

where, $\theta_{avg}$ is the mean pitch angle, $\theta_1$, $\theta_2$ and $\theta_3$ are the pitch angles of each blade and $A$ is the rotor azimuth angle.

The bending moment at the root of each blade was assumed to be measured and then transformed to d-q axis using a multi-blade coordinate transformation, as was first demonstrated by Bossanyi et al[13]. This can be applied to convert the three-phase blade root bending moments onto a 2-D perpendicular axis.

$$\begin{bmatrix} M_d \\ M_q \end{bmatrix} = \frac{2}{3} \begin{bmatrix} cos(A) & cos\left(A + \frac{2\pi}{3}\right) & cos\left(A + \frac{4\pi}{3}\right) \\ sin(A) & sin\left(A + \frac{2\pi}{3}\right) & sin\left(A + \frac{4\pi}{3}\right) \end{bmatrix} \begin{bmatrix} M_1 \\ M_2 \\ M_3 \end{bmatrix} \tag{17}$$

where $M_1$, $M_2$ and $M_3$ are the out-of-plane blade root bending moments of each blade and $M_d$ and $M_q$ are the direct and quadrature axis outputs, respectively. PI controllers were then used to control $M_d$ and $M_q$ in order to maintain the bending moments constant irrespective of changes in them due to wind shear. An inverse d-q transformation was then performed to convert the control outputs into individual blade pitch commands.

$$\begin{bmatrix} \theta_1 \\ \theta_2 \\ \theta_3 \end{bmatrix} = \begin{bmatrix} cos(A) & sin(A) \\ cos\left(A + \frac{2\pi}{3}\right) & sin\left(A + \frac{2\pi}{3}\right) \\ cos\left(A + \frac{4\pi}{3}\right) & sin\left(A + \frac{4\pi}{3}\right) \end{bmatrix} \begin{bmatrix} M_d \\ M_q \end{bmatrix} \tag{18}$$

The individual pitch command for each blade was then combined with the collective pitch command from the feedback controller. When combining FFCPC with FBIPC, the final blade pitch command was, therefore,

$$\theta_{FF\text{-}FB,i} = (P_{FB} + I_{FF\text{-}FB}) + \theta_{TFB} + \theta_{FF} + \theta_{FB,i} \tag{19}$$

where $\theta_{FB,i}$ is the FFIPC command for an individual blade, $i$, and $\theta_{FF\text{-}FB,i}$ is the combined FFCPC+FBIPC pitch command for an individual blade.

## 4.4 | Feedforward individual pitch controller

In the present study, a novel individual pitch controller was designed to tune each blade's pitch angle depending on its azimuth position. It was used to provide an additional refinement to the feedforward collective pitch controller. The approach used a 5-beam LIDAR, with beams configured as illustrated in Fig. 1. The beams were focused at 90-degree azimuthal increments, as illustrated in Fig. 3. Simulations were performed where the beams were positioned at various rotor radial span widths (30%, 50% and 70%) to determine the best-performing beam span positions for the FFCPC+FFIPC. This approach is most similar to that used by Dunne et al[17, 18], though differs in that the LIDAR beams are not rotating with the blades and the collective pitch controller is still used to provide a command to all blades. The individual feedforward pitch controller is simplistic, only requiring knowledge of the blade azimuth position and the rotor rotational speed.

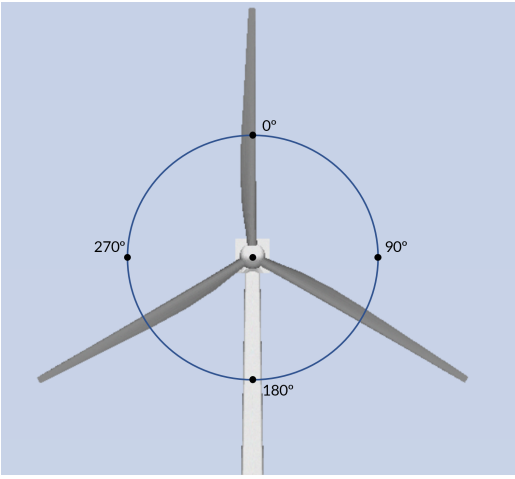


**FIGURE 3** Rotor azimuth positions of the LIDAR focal positions within the rotor plane at 50% rotor radial span.

Though the beams were focused at the specified points relative to the nacelle, the movement of the nacelle and its impact upon the measurement coordinates and beam azimuth angles were accounted for. The nacelle's (and therefore the LIDAR's) position relative to the origin was used to

modify the azimuth angles of the beams in real time. The longitudinal wind speed was recorded at each LIDAR measurement point. The pitch angle associated with the wind speed recorded by each beam was then determined through interpolation of the wind speed-pitch angle curve specified in the ROSCO input file (Fig. 2). The azimuth positions of each blade ($A_i$) at the current time were determined by feedback of the OpenFAST azimuth output ($A$).

$$A_i = A + \frac{2\pi(i-1)}{3} \tag{20}$$

where $i$ is the blade number from 1 to 3. The current rotor rotational speed ($\Omega_r$) was then used to predict the azimuth position of each blade after the specified feedforward preview time ($A_{i,new}$). An example scenario of this is illustrated in Fig. 4. This assumes that the rotor speed does not change over the preview time period.

$$A_{i,new} = A_i + \Omega_r \, t_{preview} \tag{21}$$

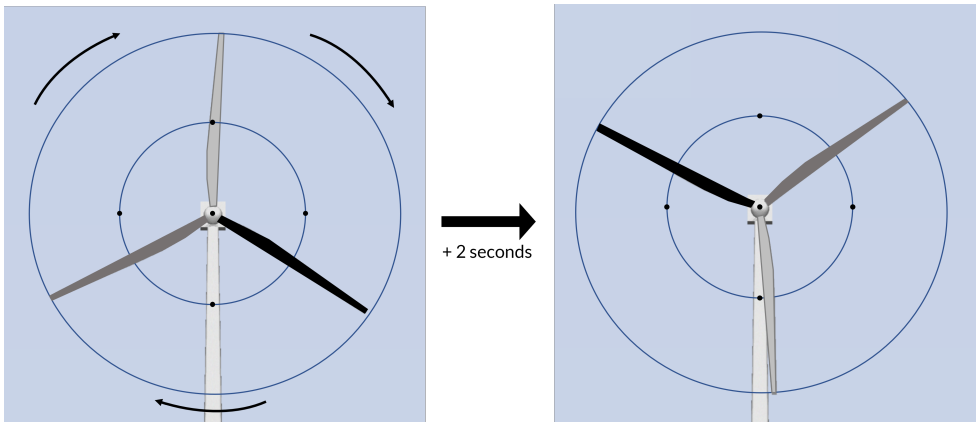


**FIGURE 4** Illustrating an example scenario of the rotation of the turbine blades during the preview time provided for the feedforward individual pitch commands.

The expected azimuth angle of each blade was then subtracted from the azimuth angle of each beam ($A_j$).

$$A_{i,dif} = A_j - A_{i,new} \tag{22}$$

where $j$ is the beam number. The beam associated with the smallest difference in azimuth angle ($A_{i,dif}$) was then selected to provide the individual pitch command to the individual blade. The error between the pitch command associated with the beam ($\theta_{FF,j}$) and the current average blade pitch angle ($\theta_{c,avg}$) was then determined.

$$e_{FF,j} = \theta_{FF,j} - \theta_{c,avg} \tag{23}$$

The error was then low-pass filtered to prevent large variations in individual pitch commands. The commands were also multiplied by a proportional gain term ($K_{p,IPC}$) to reduce the magnitude of the commands from the individual beams.

$$\theta_{FF,i} = K_{p,IPC} \, e_{FF,j} \tag{24}$$

The individual component of the controller was designed to provide small adjustments to each blade in addition to the collective command that is provided to all of the blades.

$$\theta_{FF\text{-}FB,i} = (P_{FB} + I_{FF\text{-}FB}) + \theta_{TFB} + \theta_{FF} + \theta_{FF,i} \tag{25}$$

This resulted in an individual pitch variation as shown in Fig. 5.

## 5 | SIMULATIONS

The control strategies were applied to a single turbine. Turbulent wind fields were created using TurbSim[27]. Turbulent wind fields were created with average wind speeds from 13-25 $ms^{-1}$ in intervals of 2 $ms^{-1}$, and were generated for four random seeds of 1 hour length to provide a variety of turbulent wind profiles. Four seeds were used as this provided a good balance between stochasticity and computational cost. The turbulence was

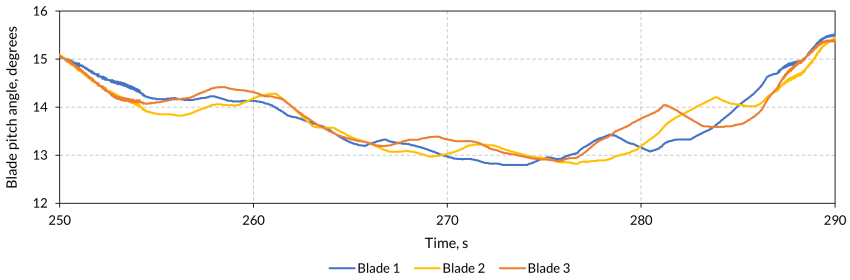


**FIGURE 5** Excerpt of time series individual blade pitch variation when using feedforward individual blade pitch control.

generated under the normal turbulence model (NTM), turbulence intensity (TI) category B[27]. These conditions fall into design load case (DLC) 1.1, as defined in the IEC standards[28]. DLC 1.1 was used as this embodies the loads resulting from turbulence that occurs during the normal operation of a wind turbine throughout its lifetime. The floating turbine was modelled in a water depth of 200 m, and under irregular waves. The wind and waves were aligned in the same direction. The significant wave height ($H_s$) and peak spectral period ($T_p$) were adjusted to suit each average wind speed integer, with values interpolated from those defined by Allen et al[10], and shown in Table 3. The LIDAR was configured to a focal distance of 200 m ahead of the turbine and measured at a rate of 4 Hz. Two seconds of preview time was provided by the feedforward commands.

**TABLE 3** IEC DLC 1.1 NTM wind and wave conditions[10].

| $U_{hub}$, $ms^{-1}$ | 13 | 15 | 17 | 19 | 21 | 23 | 25 |
|---|---|---|---|---|---|---|---|
| $H_s$, $m$ | 2.0 | 2.4 | 2.8 | 3.3 | 3.8 | 4.3 | 4.8 |
| $T_p$, $s$ | 7.5 | 7.6 | 7.8 | 8.3 | 8.8 | 9.2 | 9.7 |

## 5.1 | Statistical metrics

LIDAR-assisted pitch control is able to deliver benefits to numerous performance, loading and motion parameters of the turbine and substructure. These benefits should be assessed differently depending on the desired outcome most relevant to the parameter. The metric most commonly used when assessing the performance of LIDAR-assisted control is the standard deviation. This describes the average deviation of data points from the mean of the data set and provides knowledge of the degree of variation within the data set.

$$\sigma = \sqrt{\frac{\sum (x_i - \mu)^2}{N}} \tag{26}$$

where $\sigma$ is the standard deviation, $x_i$ is a data point, $\mu$ is the mean of the data points and $N$ is the total number of data points. A reduction in the standard deviation (compared to the baseline feedback controller) therefore indicates reduced variation in the data set and reduced magnitude of extreme values. This is particularly useful when assessing the impacts on loadings, pitch actuation mechanisms and bending moments. This is because reduced standard deviations mean that the responses are more consistent, predictable and uniform across the structure, and can result in reduced fatigue, failure rates and, therefore, lifetime extension, which can then lead to reduced maintenance activities and operational expenditure.

In above-rated wind speeds, the controller aims to maintain the rotor speed and power at 7.56 rpm and 15 MW, respectively. The root mean squared error (RMSE) metric can be applied to assess the ability of the controller to maintain the control variables at their desired set points.

$$RMSE = \sqrt{\frac{\sum (x_i - x_{setpoint})^2}{N}} \tag{27}$$

where $x_{setpoint}$ is the desired setpoint for a variable. A reduction in the RMSE of the feedforward controllers to the baseline feedback controller indicates that a variable is better controlled to its desired set point. The other metrics that were used to compare the time series results of the feedback and feedforward controllers were the ranges, maximum values and accelerations.

Table 4 highlights the key performance indicating metrics that were assessed for the various turbine and substructure parameters, with rationale explaining their significance.

**TABLE 4** Detailing the key performance indicating metrics that were assessed for the specified parameter and their significance in demonstrating the efficacy of LIDAR-assisted control.

| Parameter | Metric | Significance |
|---|---|---|
| Rotor speed | RMSE | This metric can assess how closely the rotor speed is maintained at its rated value (7.56 rpm). A lower error therefore indicates that the pitch controller is better able to deliver its control objective. |
| | Range | The range in rotor speed determines the 1P and 3P ranges, which are important for substructure and tower design. Allen et al[10] reported that for the IEA 15 MW reference turbine on the VolturnUS-S, the constraining operational rotor speed range was 3.97 to 8.86 rpm, which impacted upon the tower design. Reductions to the 1P and 3P frequency ranges may allow for the use of a soft-stiff tower, which will be a lighter and cheaper option than a stiff-stiff tower. |
| | Maximum | Floating wind turbines are prone to over-speeding by up to 30% greater than the rated rotor speed[4, 6], which can lead to shutdowns and damage to turbine components. |
| Power | RMSE | This metric can assess how closely the generator power is maintained at its rated value (15 MW). Significant variation around the setpoint can lead to excessive stress on the generator. |
| Blade pitch | $\sigma$ | A reduced standard deviation indicates a reduced degree of pitch actuation and, therefore, less demand on the pitch actuation mechanisms. |
| Thrust | $\sigma$ | A reduced standard deviation in the thrust indicates a reduction in the variation on the force applied to the wind turbine. |
| Bending moments | $\sigma$ | Reduced variation in the loadings can lead to reduced damage to turbine components, resulting in reduced failure rates, fatigue and, therefore, maintenance while allowing for structural optimisation. |
| Platform motions | $\sigma$ | Reductions to the standard deviation indicates reduced magnitude and variation of platform motions, which can improve the stability of the platform and lead to performance improvements. |
| | Acceleration (Pitch only) | Access to the turbines can be limited by the acceleration of the platform motions, primarily in pitch and, therefore, it is favourable to reduce them. |
| | Maximum (Pitch only) | The maximum magnitude of platform motions, particularly the platform pitch angle, is a design constraint for the turbine-substructure design and also limits access to the floating turbines for maintenance. |

# 6 | RESULTS AND DISCUSSION

This section presents the results of the OpenFAST simulations for the single turbine. Results are presented as normalised values, whereby the values were divided by that of the feedback-only controller.

$$X_{i,normalised} = \frac{X_i}{X_{FB}} \tag{28}$$

where $X_i$ is the value of a metric for a given parameter associated with a control strategy, $i$ (FB, FFCPC, FFCPC+FBIPC or FFCPC+FFIPC), and $X_{i,normalised}$ is the normalised value of a metric for a given control strategy. This approach allows for direct comparison to the results of the feedback controller, which are normalised to 1. Therefore, a value resulting from one of the feedforward control strategies that is less than one indicates a reduction (and therefore an improvement) compared to the baseline feedback controller and a value that is greater than one indicates an increase (and therefore a deterioration) compared to the baseline feedback controller.

## 6.1 | Feedback vs. feedforward control

This section outlines the results of the single turbine simulations. Time series results of a single seed with an average wind speed of 17 $ms^{-1}$ will be first shown, to highlight the improvements to the turbine and substructure parameters when using the collective (FFCPC) or individual feedforward pitch control (FFCPC+FFIPC) compared to the feedback-only controller. Results of the baseline feedback individual controller combined with the feedforward collective pitch controller (FFCPC+FBIPC) will also be presented to compare the effectiveness of the feedback and feedforward

individual control elements. Four seed average results from across the above-rated spectrum will then be given to further demonstrate the capability of the feedforward controllers.

### 6.1.1 | Single wind field

Figure 6 presents an excerpt of time series results of numerous turbine and substructure parameters. Within the simulations used to acquire the data for Fig. 6, the floating wind turbine was subject to a turbulent wind field with an average wind speed of 17 $ms^{-1}$ and TI category B. The substructure was modelled in an irregular wave sea state with a water depth of 200 m, $H_s$ of 2.83 m and $T_p$ of 7.85 s.

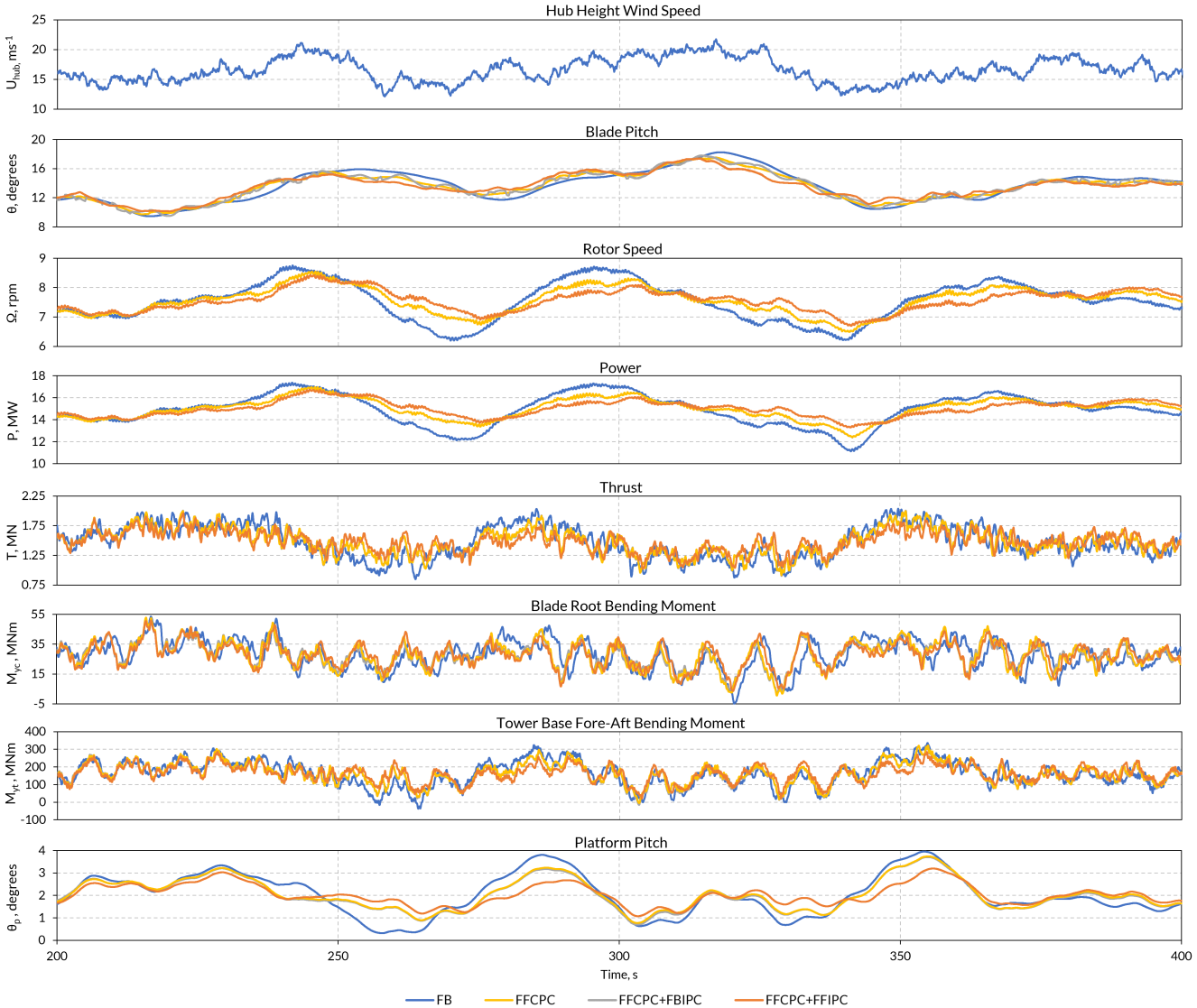


**FIGURE 6** 200-second excerpt time series results comparing the baseline FB pitch controller to the FF controllers. Simulations were performed under a turbulent wind field ($V_{avg}$ = 17 $ms^{-1}$, NTM, TI Category B) and irregular waves ($H_s$ = 2.83 m, $T_p$ = 7.85 s). The LIDAR beams were positioned at 50% rotor radial span for all feedforward control strategies.

Table 5 provides a summary of the averaged normalised metric values for various parameters delivered by the FFCPC, FFCPC+FBIPC and FFCPC+FFIPC strategies relative to the baseline feedback controller across four random seed 1-hour length simulations under the aforementioned wind and wave conditions.

**TABLE 5** Normalised metric values of various parameters through the addition of feedforward pitch control vs. baseline feedback control under a turbulent wind field ($V_{avg}$ = 17 ms$^{-1}$, NTM, TI Category B) with irregular waves ($H_s$ = 2.83 m, $T_p$ = 7.85 s). The LIDAR beams were positioned at 50% rotor radial span for all feedforward control strategies. Results shown are average normalised values across the four random seed 1-hour simulations at $V_{avg}$ = 17ms$^{-1}$.

| Parameter | Metric | Normalised FB | Normalised FFCPC | Normalised FFCPC+FBIPC | Normalised FFCPC+FFIPC |
|---|---|---|---|---|---|
| | | Performance | | | |
| | RMSE | 1.00 | 0.75 | 0.75 | 0.67 |
| Rotor speed | Range | 1.00 | 0.82 | 0.83 | 0.74 |
| | Maximum | 1.00 | 0.98 | 0.98 | 0.96 |
| Power | RMSE | 1.00 | 0.75 | 0.75 | 0.65 |
| Blade pitch | $\sigma$ | 1.00 | 0.95 | 0.96 | 0.92 |
| Thrust | $\sigma$ | 1.00 | 0.86 | 0.86 | 0.80 |
| | | Bending moments | | | |
| Blade root | $\sigma$ | 1.00 | 0.94 | 0.87 | 0.90 |
| Tower base fore-aft | $\sigma$ | 1.00 | 0.87 | 0.87 | 0.82 |
| Tower base side-to-side | $\sigma$ | 1.00 | 0.99 | 0.97 | 1.00 |
| | | Platform motions | | | |
| | $\sigma$ | 1.00 | 0.75 | 0.75 | 0.65 |
| Pitch | Acceleration | 1.00 | 0.81 | 0.81 | 0.80 |
| | Maximum | 1.00 | 0.95 | 0.94 | 0.90 |
| Roll | $\sigma$ | 1.00 | 0.99 | 0.96 | 1.01 |
| Yaw | $\sigma$ | 1.00 | 1.00 | 0.84 | 1.07 |
| Heave | $\sigma$ | 1.00 | 1.00 | 1.00 | 1.00 |
| Surge | $\sigma$ | 1.00 | 0.93 | 0.93 | 0.85 |
| Sway | $\sigma$ | 1.00 | 1.00 | 0.87 | 1.04 |

As can be seen from Fig. 6 and Table 5, the collective and individual pitch control additions are able to deliver benefits to the key metrics of numerous turbine and substructure parameters. The rotor speed and generator power benefitted most significantly, with reductions of up to 35% in the RMSEs compared to the baseline feedback controller, demonstrating improved power tracking, and reduced ranges of 1P and 3P frequencies by up to 26%. These benefits are attributed to the superior blade pitch preparation in advance of the wind's impact. This has a damping effect on the rotor's motion, thereby reducing its variation compared to the feedback-only controller. Variation in blade pitch angle is markedly reduced for all feedforward control strategies as less reactionary actuation is required compared to the feedback-only controller, indicating scope for reduced demand on the pitch actuation systems. The standard deviations of the bending moments on the blade roots and tower are also significantly reduced, attributed to the reduction in the variation of the thrust force acting on the turbine. These can lead to reductions in damage equivalent loads, failure rates and fatigue of turbine components. The variation in the blade root loads were reduced most when combining the feedforward CPC with the traditional feedback IPC (FFCPC+FBIPC) because maintaining the blade root bending moments as constant is a control objective of this approach, as was explained in Sect. 4.3. The tower base fore-aft bending moment benefitted most when combining FFCPC with FFIPC, with a reduction in the standard deviation of 18% compared to the baseline feedback controller. Similarly, in terms of platform motions, the greatest beneficiary was the pitch degree of freedom, where 25% and 35% reductions in the standard deviation compared to the baseline were recorded for FFCPC and FFCPC+FFIPC, respectively. This was expected because the thrust force reported its greatest reduction in standard deviation with FFCPC+FFIPC, meaning that a more consistent force was applied to the rotor when using feedforward control instead of feedback-only control, resulting in reduced variation in the force pushing the turbine backwards. This led to the reduced variations seen in the pitching of the platform as well as the fore-aft bending moment acting on the tower base.

Overall, the FFCPC+FFIPC strategy further enhanced the FFCPC by providing additional tuning to the pitch of the individual blades. Performance parameters benefitted most overall, with up to 10% further reductions in the RMSE of the power compared to the baseline feedback controller. The blade root and tower base fore-aft bending moments benefitted from a further 4% and 5% reduction in standard deviation compared to the baseline, respectively. The most significant improvement delivered by FFCPC+FFIPC to the platform's motions was in pitch, which achieved a further 10% reduction in standard deviation compared to the baseline feedback controller, as well as a 5% further reduction in the maximum value.

The FFCPC+FFIPC strategy was able to offer improvements upon the traditional FBIPC strategy, though both excelled in different areas. When combined with FFCPC, FFIPC gave greater improvements to the performance parameters than when FBIPC was used, while also greatly benefiting the platform pitch and surge motions in addition to the tower-base fore-aft bending moment. However, FBIPC was able to offer slight benefits over the FFIPC to the blade root and tower side-to-side bending moment as well as the yaw and sway motions of the platform.

The improvements offered by the FFCPC+FFIPC strategy over the baseline feedback control can also be illustrated by Power Spectral Density

(PSD) plots. Figure 7 presents PSD plots for the rotor speed, blade pitch, platform pitch and tower base fore-aft bending moment. The sampling frequency used in the simulations was 40 Hz and this is the maximum frequency value of the plots shown in Fig. 7.

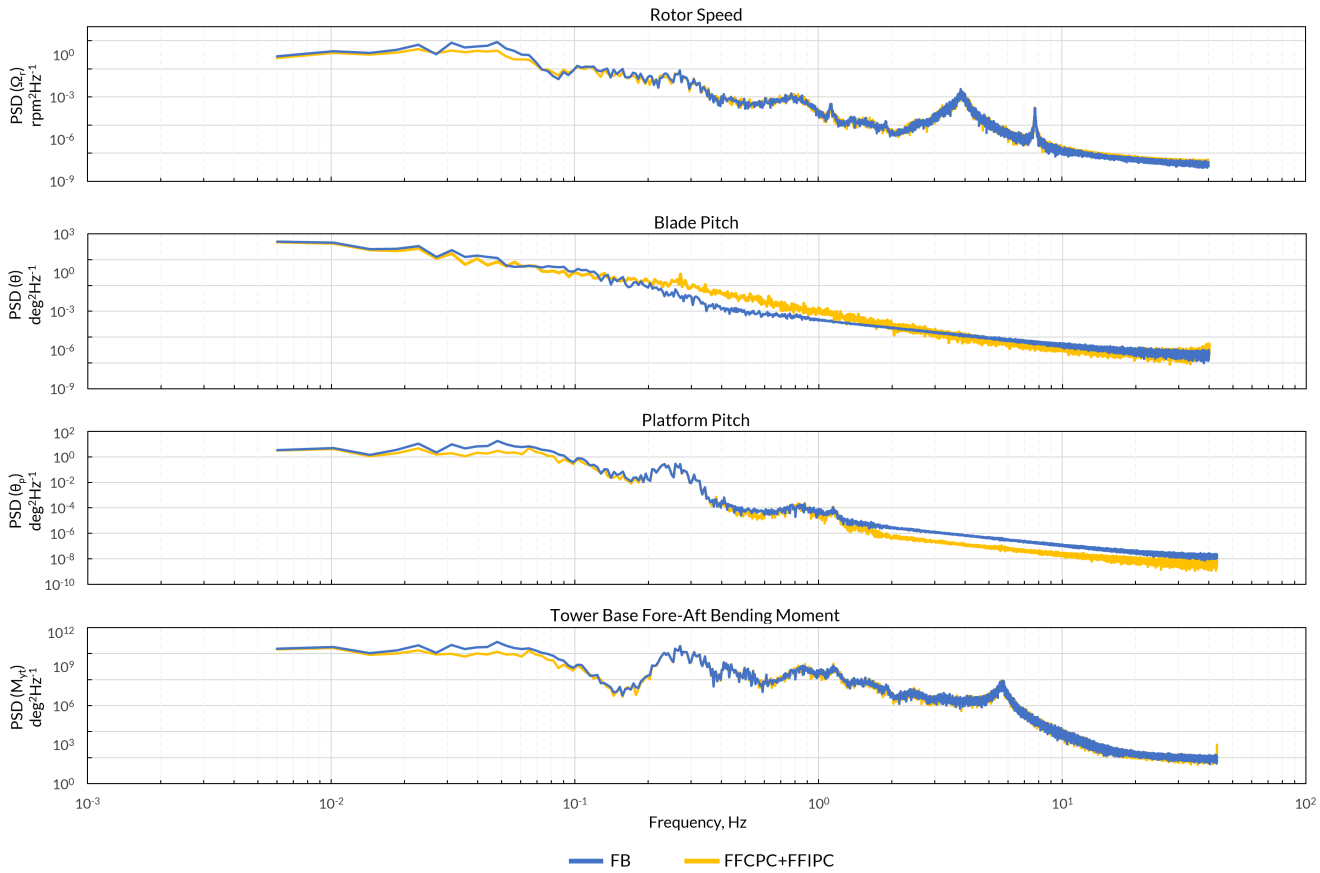


**FIGURE 7** PSD plots of the rotor speed, blade pitch, platform pitch and tower base fore-aft bending moment generated from 1 h simulations with a turbulent wind field ($V_{avg}$ = 17 ms$^{-1}$, NTM, TI Category B) and irregular waves ($H_s$ = 2.83 m, $T_p$ = 7.85 s). The LIDAR beams were positioned at 50% rotor radial span for the FFCPC+FFIPC control strategy.

The rotor speed, platform pitch and tower base fore-aft bending moment's spectra were reduced in the frequency range below the 1P range at 0.2 Hz, indicating a reduction in the influence of the wind disturbance, as was expected, and was consistent with the findings shown in Fig. 6 and Table 5. Above this frequency, the spectra for the rotor speed and tower base fore-aft bending moment when using FFCPC+FFIPC were very similar to those of the baseline controller because the feedforward pitch commands were damped out by the low pass filter. The spectrum of the blade pitch for FFCPC+FFIPC was greater than that of the baseline between the 1P and 3P ranges, which was also expected due to the additional individual control element.

### 6.1.2 | Above-rated wind spectrum

Simulations were performed across the above-rated wind spectrum from 13-25 ms$^{-1}$ in intervals of 2 ms$^{-1}$. This aimed to capture the performance benefits attainable from FFCPC with FBIPC or FFIPC across the full operating range of the pitch controller to allow for the assessment of lifetime benefits. The four seed average wind speed series results for various turbine and substructure parameters are shown in Fig. 8.

Figure 8 re-iterates the enhancements provided by the FFIPC and FBIPC controllers when combined with the FFCPC controller on its own, as these were able to deliver greater standard deviation and RMSE reductions in all parameters compared to the baseline feedback controller for the majority of the above-rated wind speeds. In general, the improvements delivered by the feedforward controllers to the turbine and substructure parameters are least significant at lower above-rated average wind speeds closer to the above-below-rated transition point (13 ms$^{-1}$ and

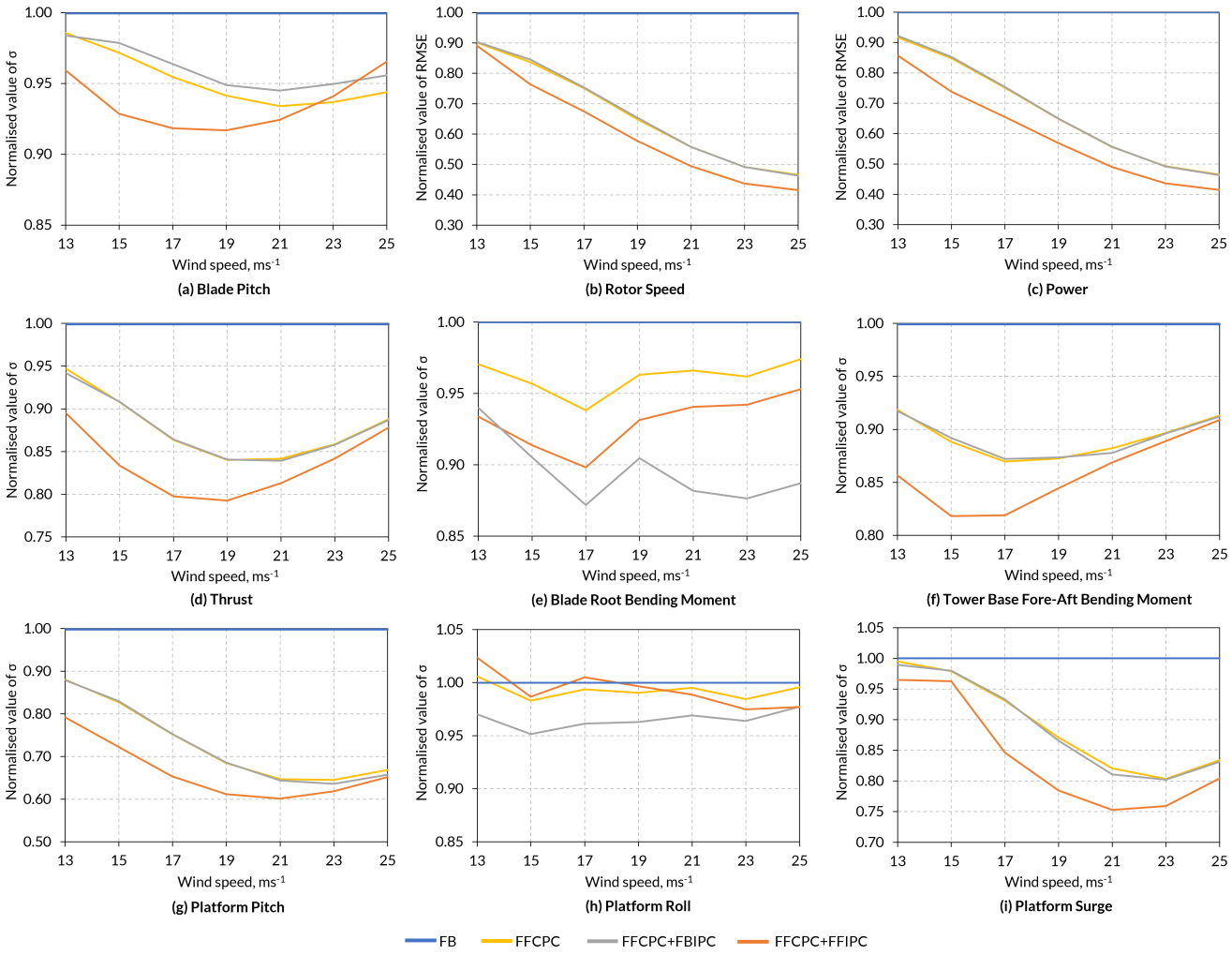


**FIGURE 8** Normalised $\sigma$ or RMSE values delivered by the feedforward controllers compared to the baseline FB-only pitch controller across the above-rated wind spectrum. The LIDAR beams were positioned at 50% rotor radial span for all feedforward control strategies. The results shown are the four seed average normalised values from the 1-hour simulations at each average wind speed integer for each control configuration.

15 ms$^{-1}$). This is because the pitch-curve of the IEA 15 MW turbine increases steeply and so limits were imposed to restrict the magnitude of the feedforward commands at these lower wind speeds. Additionally, as the wind speeds increased, some parameters experienced greater variation and higher magnitude oscillations when using the baseline feedback controller and so this led to more room for improvement for the feedforward controllers. This was particularly true for the rotor speed (Fig. 8b) and power (Fig. 8c), which benefitted most significantly, with reductions in their RMSEs by up to 58% at the highest average wind speed of 25 ms$^{-1}$. The rotor thrust (Fig. 8d) saw reductions in the standard deviation delivered by the feedforward controllers increase until approximately 19 ms$^{-1}$ before decreasing at higher wind speeds due to diminishing variation in the rotor thrust as the wind speed increased. This was mirrored within the loadings and platform motions, as reductions to the standard deviations of the tower base fore-aft bending moment (Fig. 8f), platform pitch (Fig. 8g) and platform surge (Fig. 8i) also diminished at higher wind speeds due to the decreased reduction to the standard deviation of the rotor thrust. The benefit to the blade root bending moment (Fig. 8e) remained relatively consistent across the full above-rated wind spectrum as its respective standard deviation when using the feedback and feedforward control strategies remained relatively constant as the wind speed was increased.

## 6.2 | Comparison of beam span locations

Fig. 9 shows the above-rated wind spectra results of the simulations when using beams focused at 30%, 50% and 70% rotor radial span.

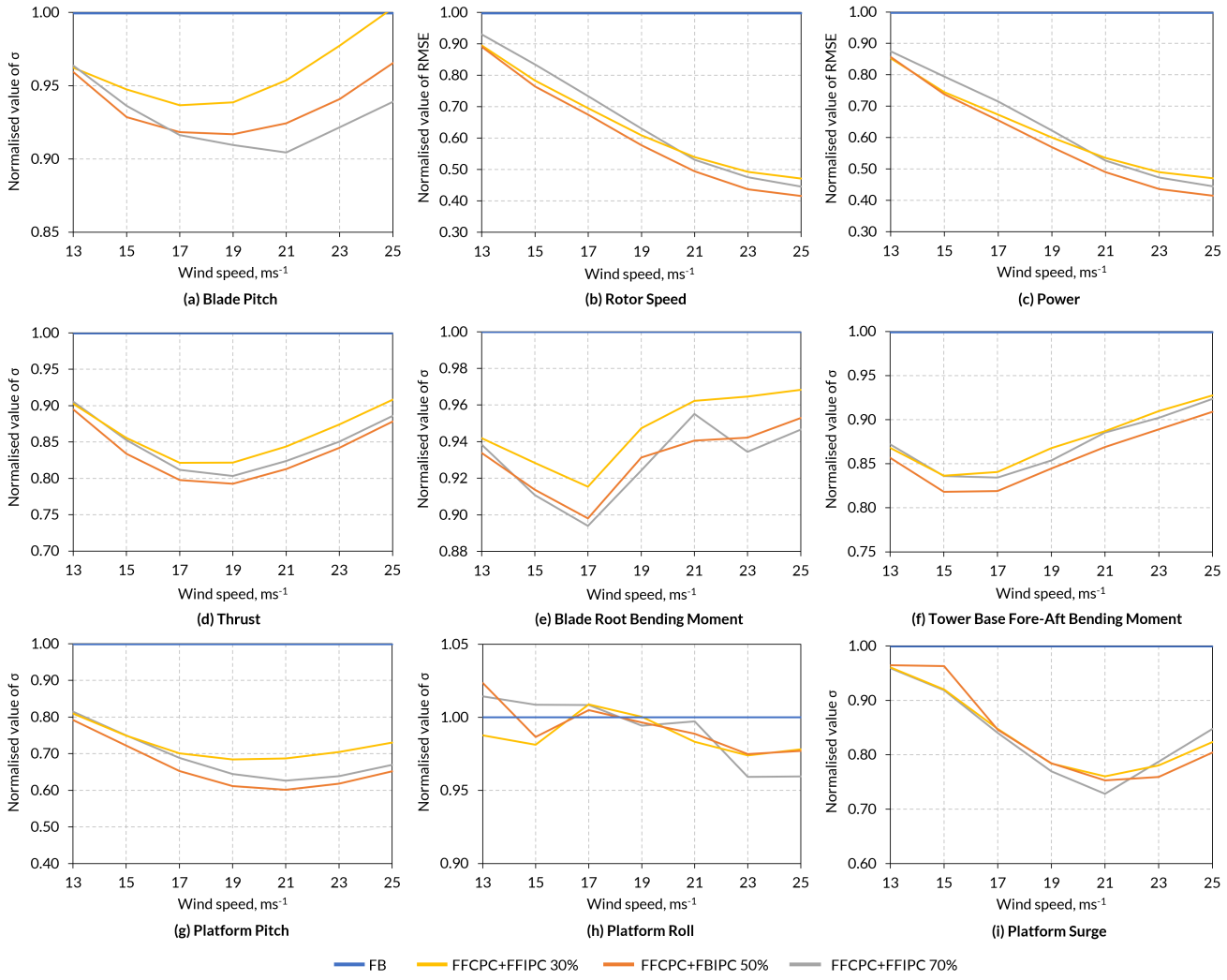


**FIGURE 9** Normalised $\sigma$ or RMSE values delivered by the FFCPC+FFIPC controller with beams positioned at 30%, 50% and 70% rotor radial span compared to the baseline feedback pitch controller across the above-rated wind spectrum. The results shown are the four seed average normalised values from the 1-hour simulations at each average wind speed integer for each control configuration.

From Fig. 9, the feedforward collective and individual controller generally performed better across the above-rated wind spectrum when the beams were focused at 50% or 70% than at 30% span. At 30% span, the benefits to the blade pitch (Fig.9a), rotor thrust (Fig.9d) and platform pitch (Fig.9g) were all less significant. The FFCPC+FFIPC performed similarly with beams positioned at 50% and 70% span. However, there were slightly greater benefits delivered when the beams were focused at 50% span compared to at 70% span, namely in the rotor speed (Fig.9b) regulation and power tracking (Fig.9c), the tower base fore-aft bending moment (Fig.9f), the rotor thrust and the platform pitch, by up to 7%.

The differences seen in the performance of the feedforward IPC at various rotor radial spans can be explained through consideration of the variation in the wind speed across the rotor-swept area as the span positions increase. At 70% span, the distance between the opposite beams was approximately 170 m, compared to 120 m at 50% span and 75 m at 30% span. As a single average wind speed was used by the feedforward collective pitch controller, the potentially larger differences in wind speed at the measurement locations impact upon the REWS used and so may lead to sub-optimal commands issued by the feedforward CPC. Similarly, at the smallest span length simulated (30%), the variation in the measured

wind velocities may not be sufficient to represent the full rotor swept area. Furthermore, for the individual control element, it is pertinent to capture the variation across the rotor-swept area in order to provide the appropriate command to the individual blades. Therefore, with the beams positioned at 50% rotor radial span, the LIDAR was able to capture the wind velocities appropriate for the effective operation of both the collective and individual feedforward pitch control elements.

## 6.3 | Study limitations

In spite of the results documented in this paper, the study is not without its limitations, which must be acknowledged. Firstly, as was discussed in Sect. 3.1, the method of obtaining the previewed wind velocity is not wholly representative of a real LIDAR system, and the wind velocity is assumed to not evolve from the point of measurement to the turbine. Furthermore, one hundred per cent LIDAR measurement availability has been assumed and the impact of blade blockage of the LIDAR beams has not been considered. Therefore, it is recommended that the results presented in this study be considered as the best-case scenario of what can be achieved through the implementation of the detailed LIDAR-assisted controllers.

Moreover, the simulations were only performed under normal operating conditions (DLC 1.1), according to the industrial standards [28]. Therefore, the scope of this study does not account for extreme operating conditions and gusts.

Finally, it is uncertain whether the control methodology used within this work is directly transferable to current commercial floating offshore wind turbine controllers due to a lack of available knowledge of their operation within the public domain.

# 7 | CONCLUSIONS

This study has presented a novel LIDAR-assisted feedforward individual pitch control approach in combination with a feedforward collective pitch control strategy. This was applied to the IEA-Wind 15 MW reference turbine mounted on the UMaine VolturnUS-S semi-submersible floating substructure. The benefits of the feedforward IPC were investigated using modified versions of the OpenFAST and ROSCO. LIDAR simulation was added to the OpenFAST program through modification to the source code of the InflowWind module. The changes made are now present in the latest release of OpenFAST, v3.5. LIDAR measurements were then interfaced to ServoDyn to allow for transfer to ROSCO for LIDAR-assisted control, where code for collective and individual feedforward pitch control was incorporated. The results presented demonstrate the efficacy of the LIDAR simulation and control additions to OpenFAST and ROSCO and can serve as a demonstration of the capabilities of the LIDAR simulation available in OpenFAST v3.5.

Simulations were performed on a single floating turbine, which yielded significant time series standard deviation, root mean squared error, range and maxima reductions for both collective and individual feedforward controllers over the baseline feedback collective and individual controllers. The individual feedforward pitch controller was able to provide enhancement to the collective feedforward pitch controller through increased standard deviation reductions over the baseline feedback controller by up to 10% at an average wind speed of 17 $ms^{-1}$. Simulations were performed to cover the full above-rated wind spectrum, which highlighted that standard deviation and root mean squared error reductions delivered by the feedforward controllers generally increased with increasing wind speed. The feedforward collective combined with the feedforward individual controller was found to give the greatest benefits over the baseline feedback controller, primarily in the rotor speed, power, platform pitch and tower base fore-aft bending moment, due to the wind speed-azimuth focused tuning of the blade pitch. The combined feedforward collective and individual pitch controller was studied at multiple rotor radial percentage span locations. The controller was found to perform best when the beams were focused at 50% span, offering the best balance between the rotor effective average wind speed used by the collective control element whilst capturing the variation across the rotor swept area used for the individual control component.

Future work aims to assess the variation in the performance of the feedforward IPC when accounting for the variation in the rotor speed during the preview time interval and the performance when zero difference in azimuth position to the blades is used. Following this study, future work also aims to extend the scope of the research to the array level using FAST.Farm. Lifetime operations and maintenance cost reductions of the floating offshore wind turbines will also be quantified through assessment of the lifetime failure rate and damage equivalent load reductions. Further work will also aim to investigate the potential for structural optimisation of the tower given the LIDAR-assisted controller's ability to reduce the range in the rotor speed and therefore the 1P and 3P frequency ranges.

## AUTHOR CONTRIBUTIONS

**Andrew Russell** conceived the concept, performed the modifications to the OpenFAST and ROSCO source codes, executed the simulations and prepared the paper. **Maurizio Collu, Alasdair McDonald, Philipp Thies, Aidan Keane** and **Alexander Quayle** provided supervision, suggestions and reviewed the paper.

## ACKNOWLEDGMENTS

This work was funded by UK Research and Innovation as part of the EPSRC and NERC Industrial CDT for Offshore Renewable Energy (IDCORE), Grant number EP/S023933/1.

The authors wish to acknowledge the support provided by NREL, namely Andy Platt and Derek Slaughter, for facilitating the integration of the proposed changes into OpenFAST v3.5.

## CONFLICT OF INTEREST

The authors declare no potential conflict of interest.

## DATA AVAILABILITY STATEMENT

The original modified version of OpenFAST v.3.4, which includes the LIDAR simulator used in this work can be accessed via https://github.com/Russell9798/OpenFAST-v3.4-Lidar-IfW-Original/releases/tag/1.0, https://doi.org/10.5281/zenodo.7956023. The modified version of ROSCO v2.6 with the feedforward control additions can be accessed via https://github.com/Russell9798/ROSCO-v2.6-LAC-IPC/releases/tag/1.1, https://doi.org/10.5281/zenodo.7955992.

Simulation datasets used for this paper are available and can be assessed via https://zenodo.org/record/8192801, https://doi.org/10.5281/zenodo.8192801.

## ORCID

Andrew Russell - https://orcid.org/0009-0008-2534-7664

## REFERENCES

1. Schlipf D, Simley E, Lemmer F, Pao L, Cheng PW. Collective pitch feedforward control of floating wind turbines using LIDAR. In: 25th ISOPE International Ocean and Polar Engineering Conference. 2015:ISOPE-I-15-755.
2. Navalkar S, Wingerden vJ, Fleming PA, Van Kuik G. Integrating robust LIDAR-based feedforward with feedback control to enhance speed regulation of floating wind turbines. In: 2015 American Control Conference (ACC). 2015:3070–3075. doi: 10.1109/ACC.2015.7171804
3. Schlipf D, Lemmer F, Raach S. Multi-variable feedforward control for floating wind turbines using LIDAR. In: 30th ISOPE International Ocean and Polar Engineering Conference. 2020:ISOPE-I-20-1174.
4. Larsen T, Hanson T. A method to avoid negative damped low frequent tower vibrations for a floating, pitch controlled wind turbine. *Journal of Physics: Conference Series*. 2007;75(1):012073. doi: 10.1088/1742-6596/75/1/012073
5. Yu W, Lemmer F, Schlipf D, et al. Evaluation of control methods for floating offshore wind turbines. *Journal of Physics: Conference Series*. 2018;1104(1):012033. doi: 10.1088/1742-6596/1104/1/012033
6. Fischer B. Reducing rotor speed variations of floating wind turbines by compensation of non-minimum phase zeros. *IET Renewable Power Generation*. 2013;7(4):413–419. doi: 10.1049/iet-rpg.2012.0263
7. Jonkman J, Butterfield S, Musial W, Scott G. Definition of a 5-MW reference wind turbine for offshore system development. Tech. Rep. NREL/TP-500-38060, NREL, Golden, CO (US). 2009. doi: 10.2172/947422
8. MingYang . Leading innovation: MingYang Smart Energy launches MySE 16.0-242, the world's largest offshore Hybrid Drive wind turbine. 2021. URL: http://www.myse.com.cn/en/jtxw/info.aspx?itemid=825.
9. Gaertner E, Rinker J, Sethuraman L, et al. Definition of the IEA-Wind 15-Megawatt offshore reference wind turbine. Tech. Rep. NREL/TP-5000-75698, NREL, Golden, CO. 2020. doi: 10.2172/1660012
10. Allen C, Viscelli A, Dagher H, et al. Definition of the UMaine VolturnUS-S reference platform developed for the IEA-Wind 15-Megawatt offshore reference wind turbine. Tech. Rep. NREL/TP-5000-76773, NREL, Golden, CO (US). 2020. doi: 10.2172/1660012
11. Schlipf D, Guo F, Raach S, Lemmer F. A tutorial on LIDAR-assisted control for floating offshore wind turbines. In: 2023 American Control Conference (ACC). 2023:2536–2541. doi: 10.23919/ACC55779.2023.10156419
12. Guo F, Schlipf D. Assessing LIDAR-assisted feedforward and multivariable feedback controls for large floating wind turbines. *Wind Energy Science Discussions*. 2023;2023:1–25. doi: 10.5194/wes-2023-9
13. Bossanyi EA. Individual blade pitch control for load reduction. *Wind Energy*. 2003;6(2):119–128. doi: 10.1002/we.76
14. Namik H, Stol K. Individual blade pitch control of floating offshore wind turbines. *Wind Energy*. 2010;13(1):74–85. doi: 10.1002/we.332
15. Schlipf D, Schuler S, Grau P, Allgöwer F, Kühn M. Look-ahead cyclic pitch control using LIDAR. University of Stuttgart. 2010. doi: 10.18419/opus-4538

16. Raach S, Schlipf D, Sandner D, Cheng PW. Nonlinear model predictive control of floating wind turbines with individual pitch control. In: 2014 American control conference (ACC). 2014:4434–4439. doi: 10.1109/ACC.2014.6858718

17. Dunne F, Pao L, Wright A, Jonkman B, Kelley N. Combining standard feedback controllers with feedforward blade pitch control for load mitigation in wind turbines. In: 48th AIAA aerospace sciences meeting including the new horizons forum and aerospace exposition. 2010:250. doi: 10.2514/6.2010-250

18. Dunne F, Schlipf D, Pao L, et al. Comparison of two independent LIDAR-based pitch control designs. In: 50th AIAA Aerospace Sciences Meeting Including the New Horizons Forum and Aerospace Exposition. 2012:1151. doi: 10.2514/6.2012-1151

19. NREL . OpenFAST v3.5.0. 2023. URL: https://github.com/OpenFAST/openfast/releases/tag/v3.5.0.

20. Abbas NJ, Zalkind DS, Pao L, Wright A. A reference open-source controller for fixed and floating offshore wind turbines. *Wind Energy Sci.*. 2022;7(1):53–73. doi: 10.5194/wes-7-53-2022

21. NREL . OpenFAST v3.4.0. 2022. URL: https://github.com/OpenFAST/openfast/tree/v3.4.0.

22. Schlipf D, Trujillo JJ, Basterra V, Kühn M. Development of a wind turbine LIDAR simulator. University of Stuttgart. 2009. doi: 10.18419/opus-3914

23. Guo F, Schlipf D, Zhu H, Platt A, Cheng PW, Thomas F. Updates on the OpenFAST LIDAR simulator. *Journal of Physics: Conference Series*. 2022;2265(4):042030. doi: 10.1088/1742-6596/2265/4/042030

24. Guo F, Schlipf D, Cheng P. Evaluation of LIDAR-assisted wind turbine control under various turbulence characteristics. *Wind Energy Sci.*. 2023;8(2):149–171. doi: 10.5194/wes-8-149-2023

25. Taylor G. The spectrum of turbulence. *Proceedings of the Royal Society of London. Series A-Mathematical and Physical Sciences*. 1938;164(919):476–490. doi: 10.1098/rspa.1938.0032

26. Magar KT, Balas MJ, Frost S. Direct adaptive control for individual blade pitch control of wind turbines for load reduction. *Journal of Intelligent Material Systems and Structures*. 2015;26(12):1564–1572. doi: 10.1177/1045389X14566527

27. Kelley ND, Jonkman BJ. Overview of the TurbSim stochastic inflow turbulence simulator. Tech. Rep. NREL/TP-500-36971, NREL, Golden, CO (US). 2005. doi: 10.2172/15020329

28. IEC 61400-3-1:2019 - Wind energy generation systems - Part 3-1: Design Requirements for fixed offshore wind turbines. Tech. Rep. British Standards Institution, London, UK. 2019.